FINITE ELEMENT SIMULATION OF A MAGNETIC BRAKE WITH A SOFT MAGNETIC SOLID IRON ROTOR

Herbert De Gersem and Kay Hameyer

Katholieke Universiteit Leuven, Dep. EE (ESAT) / Div. ELEN
Kardinaal Mercierlaan 94, B-3001 Leuven, Belgium, e-mail: Herbert.DeGersem@esat.kuleuven.ac.be

***Abstract* — A magnetic brake with a solid iron cylinder rotating at high speeds is considered. The rotor iron is both conductive and permeable. The magnetisation curve is non-linear. Special attention is paid to the correct integration of the angular velocity term. A Newton-Raphson scheme dealing with the non-linear material characteristics, is applied. The numerical oscillations appearing in the finite element model at high velocities are overcome by an adaptive mesh refinement technique combined with the artificial diffusion upwind technique. End effects due to the finite length of the rotor are incorporated by an electric circuit coupling. Simulations are performed to study the influence of the saturation of the moving rotor upon the speed-torque characteristic of the magnetic brake. It is remarkable that in the case of this solid rotor magnetic brake, the saturation of the rotor iron has a beneficial influence on the device performance.**

I. INTRODUCTION

A rotational magnetic brake consists of a stator yoke with four poles and a solid iron rotor (Fig. 2). The stator windings excite a four-pole DC air gap magnetic field. The rotor is a conductive solid iron cylinder. The magnetic properties of the iron are highly non-linear. The symmetry of the geometry and the excitation enables the application of a reduced model considering one pole pitch with periodical boundary conditions (Fig. 2). Because the material distribution and the excitation of a solid rotor do not depend on its angular position, the rotor is said to be *uniform* with respect to rotation. This considerably simplifies the simulation because motional eddy current effects can be accounted for by adding a motional eddy current term to the Maxwell equations. Hence, the application of expensive time stepping and moving mesh techniques is avoided.

In order to enable the simulation of technical devices, classical finite element simulation techniques for moving conductors have to be adopted at several points [1,2,3,4,5]. The motional finite element approach, summarised in Section 2, is accomplished by a field-circuit coupling approach (Section 3), a combined upwind, adaptive mesh refinement strategy (Section 4) and a non-linear iteration (Section 5). The circuit coupling is necessary to model the end effects introduced by the finite length of the rotor. The combination of upwinding and adaptive mesh refinement overcomes numerical oscillations occurring at high velocities. The non-linear scheme accounts for the saturation of the soft magnetic rotor and stator parts. These extended features ensure an efficient application of motional finite element simulation to a DC magnetic brake as shown in Section 6.

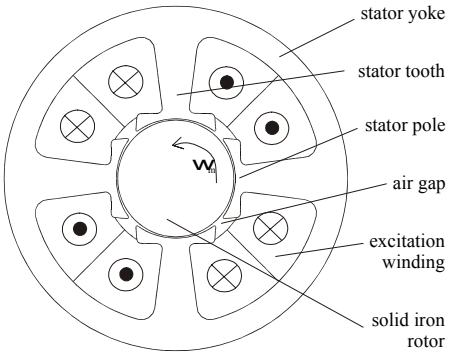

Fig. 2. Rotational magnetic brake.

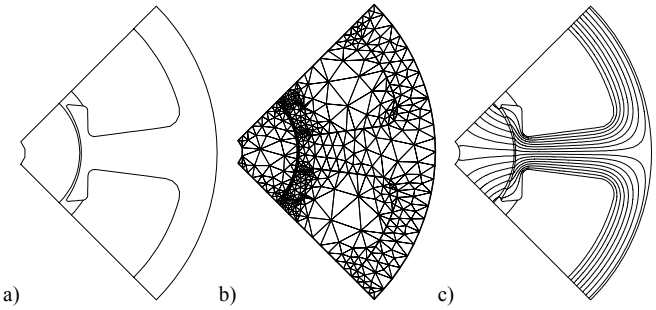

Fig. 2. a) One-pole model; b) initial mesh; c) magnetic flux line plot at standstill excited by 1 A.

II. MAGNETIC FINITE ELEMENT MODEL

It is a common practice to simulate rotating electrical devices by 2D FE models [6]. Hence, a DC magnetic brake can be modelled by the 2D static motional formulation

$$-\nabla\cdot\left(\nu\nabla A_z\right)+\sigma\mathbf{v}\cdot\nabla A_z=\sigma\frac{\Delta V}{\ell_z} \qquad (1)$$

with A_z the z-component of the magnetic vector potential, ν the reluctivity, σ the conductivity, $\mathbf{v}$ the velocity, ΔV the voltage drop between the front and the rear end of the model and ℓ_z the model length. Linear finite elements $N_i(x,y)$ are defined at the vertices of a triangulation of the device cross-section. The Galerkin procedure yields the system of equations

$$\left[k_{ij} + m_{ij}\right]\left[A_{zj}\right] = \left[t_i\right] \tag{2}$$

to be solved for the potentials A_{zj} defined at the vertices. The right hand side is

$$t_i = \underbrace{\int_\Omega \frac{\sigma}{\ell_z} N_i d\Omega}_{p_i} \Delta V \,. \tag{3}$$

The coefficients

$$k_{ij} = \int_\Omega \nu \nabla N_i \cdot \nabla N_j d\Omega \,; \tag{4}$$

$$m_{ij} = \int_\Omega \sigma \mathbf{v} \cdot \nabla N_j N_i d\Omega \tag{5}$$

represent diffusion and convection respectively. In this case, the velocity is not constant and a careful integration of (5) is required. In the case of angular motion, the velocity is linearly dependent on the radius. A convenient scheme consists of expressing the velocity as a linear combination of the velocities $\mathbf{v}_p$ at the corner nodes of the elements:

$$\mathbf{v} = \sum_{p=1}^{3} \mathbf{v}_p N_p \,. \tag{6}$$

Eq. (5) is then evaluated by

$$m_{ij} = \sum_{e=1}^{n_e} \sum_{p=1}^{3} \int_{\Omega_e} \sigma \mathbf{v}_p \cdot \nabla N_j N_i N_p d\Omega \tag{7}$$

with Ω_e the support of a single element and n_e the number of elements.

The system of equations (2) is sparse and not symmetric. The system is iteratively solved by the Bi-Conjugate Gradient method or the Generalised Minimal Residual method [7]. To achieve an acceptable convergence, (2) is preconditioned by Successive Over-Relation.

III. EXTERNAL ELECTRIC CIRCUIT MODEL

Because the stator is excited by a DC source and because the velocity of the rotor is assumed to be constant, the excitation voltages can be computed in advance. The electric behaviour of the rotor, however, depends upon the magnetic field. If a known voltage is applied across the solid rotor, the right hand side of (2) would be completely determined. Here, however, the rotor is connected in series with an additional resistor R_{add} modelling the current closing path at the front and rear ends of the device (Fig. 3). The periodicity of the model is reflected in the network by the short-circuit connection of the front and rear ends [9]. The voltage across the rotor is treated as an additional unknown ΔV_r. The z-component of the current density in the moving rotor is

$$J_z = \sigma \frac{\Delta V_r}{\ell_z} - \sigma \mathbf{v} \cdot \nabla A_z \,, \tag{8}$$

with the second part representing the motional eddy current density. The current through the rotor cross-section Ω_r follows by integrating (8) and applying the finite element unknowns A_{zj}:

$$I_r = \underbrace{\int_{\Omega_r} \frac{\sigma}{\ell_z} d\Omega}_{G_r} \Delta V_r - \sum_j A_{zj} \underbrace{\int_{\Omega_r} \sigma \mathbf{v} \cdot \nabla N_j d\Omega}_{q_{rj}} \,. \tag{9}$$

The Kirchhoff current law applied to a node of the rotor circuit gives rise to additional equation in the system matrix:

$$\begin{bmatrix} k_{ij} + m_{ij} & p_{ir} \\ -q_{rj} & G_r + \dfrac{1}{R_{add}} \end{bmatrix} \begin{bmatrix} A_{zj} \\ \Delta V_r \end{bmatrix} = \begin{bmatrix} t_i \\ 0 \end{bmatrix} . \tag{10}$$

A strong field-circuit coupled approach, i.e., combining field and circuit models in a single system matrix, is preferred in order to achieve an acceptable simulation speed. The treatment of more general circuits coupled to a finite element model is described in [8].

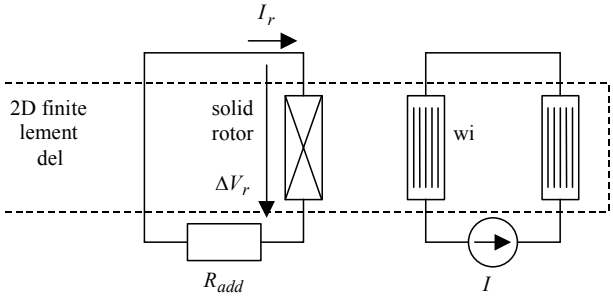

Fig. 3. Field-circuit coupled model with solid rotor, stator windings, current source and additional rotor resistor.

IV. UPWINDING

At high speeds, deteriorated solutions are observed (Fig. 4). The oscillations present in the finite element solution have a non-physical nature and are related to the discretisation technique [10]. For high velocities, the convection in the model becomes dominant over the diffusion. If for a given discretisation with the characteristic mesh size h, the Péclet number

$$Pe = \frac{h\sigma\|\mathbf{v}\|}{2\nu} \tag{11}$$

exceeds 1, numerical instabilities may occur when applying the standard Galerkin discretisation technique [11]. By simulating motional models, it is crucial to detect these numerical problems and to cope with them. In Fig. 4, it is

obvious that the field solution is wrong. The accuracy of the solution may, however, already be unacceptable even if no oscillations are visible.

Requiring that $Pe < 1$ for each element of the finite element mesh, is a sufficient to ensure a stable solution for a given mesh. A mesh violating this condition, however, may still provide an accurate solution as long as the elements for which $Pe < 1$ are located in regions with a relatively low magnetic flux density. Imposing $Pe < 1$ for a linear finite element discretisation requires decreasing the characteristic mesh size h or decreasing the ratio $\sigma\|\mathbf{v}\|/2\nu$, thus decreasing the importance of the convection relatively to the diffusion or a combination of both. The first approach may lead to unacceptable huge models and simulation times whereas the second approach involves the change of the original differential problem.

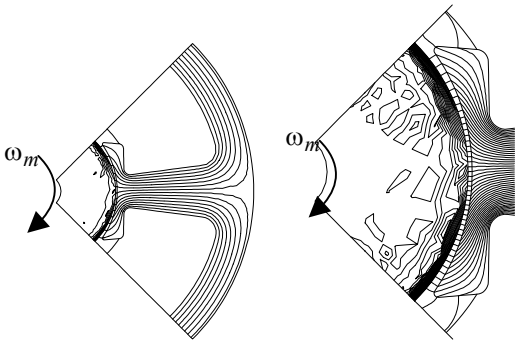

Fig. 4. Finite element solution suffering from numerical oscillations (linear material, angular velocity -100 rad/s).

The a-priori refinement of the mesh until $Pe < 1$ for all elements involves an unacceptable amount of finite element degrees of freedom on places in the model where it is not required. The application of adaptive mesh refinement depends upon the availability of reliable intermediate solutions, even on rough meshes [12]. An error estimator interpreting a solution as shown in Fig. 4, would advice the mesh refinement algorithm to add elements on not appropriate places. Stable intermediate solutions are ensured by applying the second approach. An extra amount of artificial diffusion

$$\nu_{add} = \frac{h\sigma\|\mathbf{v}\|}{2} \tag{12}$$

is added to the diffusion terms of (2). Because this intervention changes the differential problem itself, the obtained solution does not reflect the true behaviour of the device [13]. The altered model has however the property to provide stable solutions to which adaptive refinement is applicable. The error estimator marks the elements with high Péclet numbers and those with high magnetic energies. The refinement decreases the mesh size only at places of interest. The combined approach favours transition zones in the convective regions (Fig. 5). After a few steps of refinement, the need for upwinding has diminished and does only exist at places where the magnetic field is not important for the overall model behaviour.

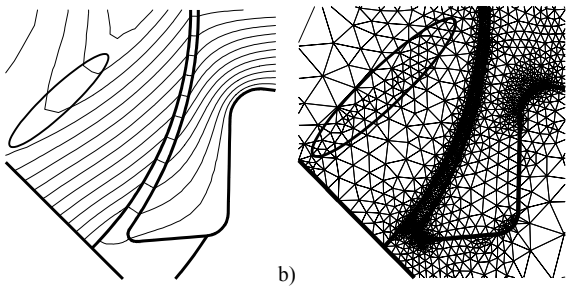

Fig. 5. Detail of a magnetic flux line plot (a) corresponding to a refined mesh (b), the ellips indicates a transition layer.

V. NEWTON-RAPHSON ITERATION

The finite element simulation deals with the non-linear magnetisation characteristic of the stator and rotor iron by a Newton-Raphson iterative scheme. The Jacobian of the finite element discretised partial differential equation at the *(n)*th iteration step is

$$\lfloor k_{ij} + p_{ij} + m_{ij} \rfloor \tag{13}$$

with

$$p_{ij} = \int_{\Omega} \frac{\partial \nu}{\partial\left(|B|^2\right)} \nabla A_z^{(n)} \cdot \nabla N_i \nabla A_z^{(n)} \cdot \nabla N_j d\Omega \,. \tag{14}$$

The magnetisation characteristic is optimised to ensure a monotonically increasing reluctivity. The technically smooth curve yields an optimal convergence of the Newton-Raphson scheme [14].

VI. APPLICATION

The numerical techniques described in this paper are applied to a DC rotational magnetic brake, excited by a DC current source. The DC current excitation of the stator windings causes a standstill field in the device (Fig. 6a). Due to the motion of the conductive rotor through the field, currents are induced therein generating a reaction field (Fig. 6b). The resulting magnetic field shows a flux pattern that is swept along in the direction of the rotation (Fig. 6c).

In order to study the influence of the non-linear permeability of the rotor iron upon the torque excited by the magnetic brake, a second, fictitious model is built by replacing the rotor iron by an equivalent linear material, featuring the same permeability at low fields but without saturation at higher fields. In Fig. 7, both models are simulated for different angular velocities. As the speed increases (from left to right in Fig. 7), the magnetic flux lines are pushed towards the surface of the solid iron rotor. In the non-linear model (under in Fig. 7), it is not possible to built up such a dense flux pattern at the rotor surface because of the non-linearity of the material. The flux is redistributed towards the inside of the rotor (Fig. 7e) or at large velocities towards the air gap of the device (Fig. 7f).

The torque excited by the brake depends on the rate of flux coupled between the stator and the rotor. As the non-linearity of the model has a significant influence on the flux pattern, the torque is also largely influenced by the saturation. In general, the torque is quadratically related to the excitation

current. For a rotor operated at -50 rad/s, the non-linear model establishes higher torques compared to the linear model. It is however not obvious that this conclusion is valid for all speed ranges. For -10 rad/s, the non-linear model seems to include more coupled flux than the linear one (compare Fig. 7e to Fig. 7b) whereas for -100 rad/s, the situation shows the opposite behaviour.

The torque is calculated by the Maxwell stress tensor method. To ensure the highest possible accuracy, the enhanced approach described in [15] is used. For the both models considered here, the speed-torque characteristic shows a raising torque related to the increasing electromotive force for increasing velocities. The non-linear model yields higher torques when compared to the linear model. This is an unexpected result. Commonly, ferromagnetic saturation tends to decrease the performance of technical devices. To validate the simulation results, a comparison with a simplified analytical model is offered. The data used in the analytical model are as close as possible to those of the true device (Table 1). Only the moving rotor is considered. The magnetic field excited by the stator is applied as a boundary condition. The analytical solution for A_z in a cylinder with radius r_0, permeability μ and conductivity σ rotating at the angular velocity ω_m in a homogeneous field $A_z(r_0,\theta) = \hat{A}_z \cos\theta$ is

$$A_z(r,\theta) = \mathrm{Re}\left\{ \hat{A}_z \frac{I_1(\xi r)}{I_1(\xi r_0)} e^{j\theta} \right\} \qquad (15)$$

with $\xi = \sqrt{j\omega_m \sigma \mu}$ and I_1 the modified Bessel function of the first kind and of first order. The torque excited on the cylinder is

$$T = \frac{\ell_z 2\pi \hat{A}_z^2}{\mu} \mathrm{Im}\left\{ \frac{\xi r_0 I_2(\xi r_0)}{I_1(\xi r_0)} \right\}. \qquad (16)$$

The evaluation of (16) for different values of ω_m shows a good qualitative agreement with the numerically obtained results (Fig. 10). The speed-torque characteristic shifts to above if μ is decreased. Due to saturation, the permeability of the rotor material decreases and hence, a higher torque is to be expected. This effect is opposite to the fact that increasing the permeability of the iron of a slotted rotor improves the machine behaviour. For this solid rotor case, the complicated interplay of magnetic diffusion and motional eddy current effects is responsible for this unexpected behaviour. The fact that the difference between linear and non-linear simulation is so large, indicates that the surface of the solid rotor is significantly saturated. The comparison of the non-linear with the linear model indicates that ferromagnetic saturation has a large influence on magnetic brake performance and that ferromagnetic saturation can not be neglected in the simulation of magnetic brakes with iron rotors.

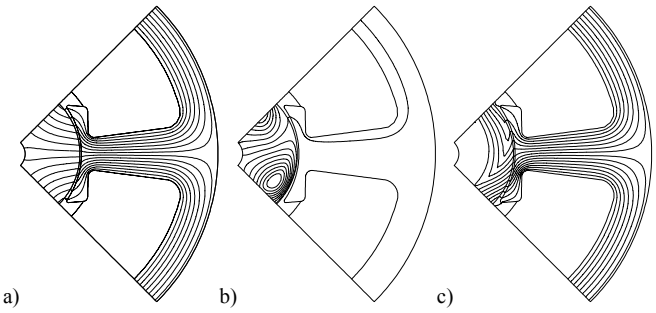

Fig. 6. Magnetic flux lines plots of (a) the field excited by the stator supply, (b) the field excited by the induced rotor currents and (c) the total field in the device (non-linear model excited by 15 A and rotating at -50 rad/s).

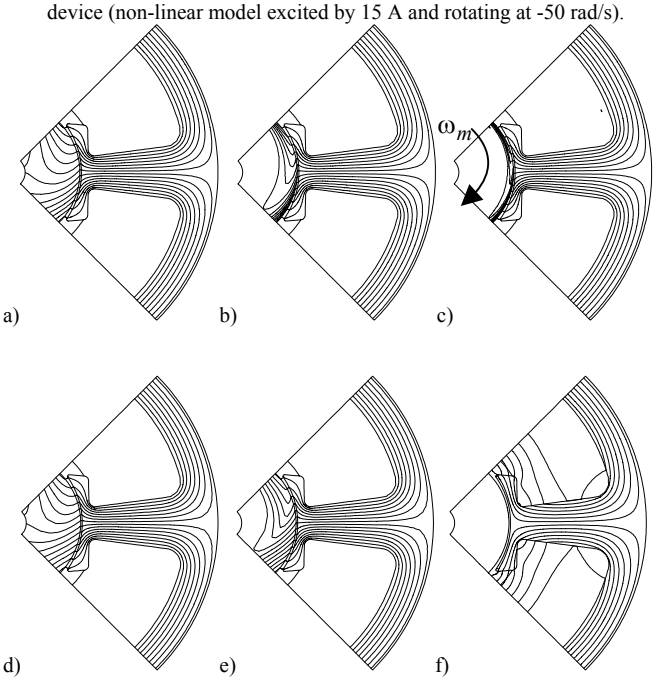

Fig. 7. Magnetic flux line plots of the linear (a,b,c) and non-linear (d,e,f) simulations of the magnetic brake with the stator excited by 15 A and the rotor rotating at 1 rad/s (a,d), 10 rad/s (b,e) and 100 rad/s (c,f).

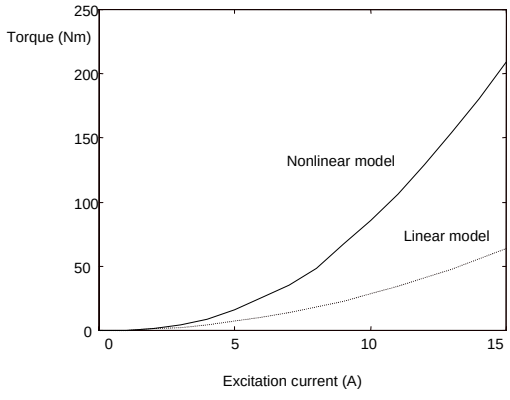

Fig. 8: Current-torque characteristics of the magnetic brake rotating at -50 rad/s in the case of linear rotor iron and in the case of non-linear rotor iron.

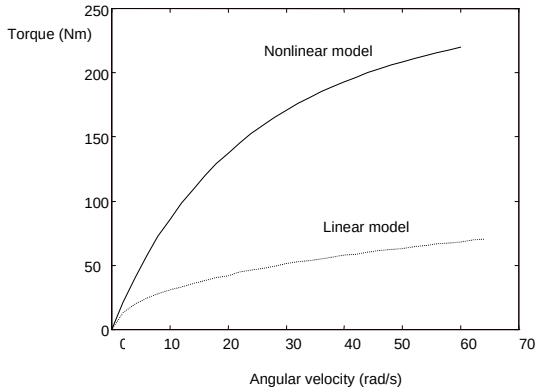

Fig. 9. Speed-torque characteristics of the magnetic brake excited by 15 A in the case of linear rotor iron and in the case of non-linear rotor iron.

Table I. Data used in the analytical model.

radius rotor	r_0	44 mm
conductivity rotor iron	σ	2.0e06 S/m
permeability rotor iron	μ	1624 μ_0
device length	ℓ_z	100 mm
applied stator field	$\hat{A}_z$	1.0e-3 Tm
velocity	ω_m	0-100 rad/s

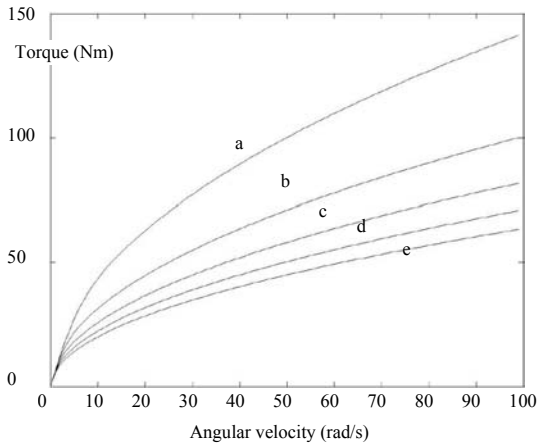

Fig. 10. Speed-torque characteristics of an analytical model for a rotating cylinder. The permeability of the rotor iron is (a) 300 μ_0 ; (b) 600 μ_0 ; (c) 900 μ_0 ; (d) 1200 μ_0 ; (e) 1500 μ_0 .

VII. CONCLUSIONS

A finite element tool simulating eddy current effects due to motion is equipped with careful integration of the velocity terms in the case of rotational motion, with adaptive mesh refinement to obtain an accurate final solution, with upwinding to ensure stable intermediate solutions and with a Newton-Raphson iteration scheme dealing with the non-linear material properties. The approach presented here enables the simulation of magnetic brakes rotating at high velocities. The influence of the non-linearity of the rotor iron on the speed-torque characteristic is studied.

ACKNOWLEDGEMENT

The authors are grateful to the Belgian "Fonds voor Wetenschappelijk Onderzoek Vlaanderen" (project G.0427.98) for its financial support of this work and the Belgian Ministry of Scientific Research for granting the IUAP No. P4/20 on Coupled Problems in Electromagnetic Systems. The research Council of the K.U.Leuven supports the basic numerical research.

REFERENCES

[1] Y. Marechal, G. Meunier, “Computation of 2D and 3D eddy currents in moving conductors of electromagnetic retarders”, *IEEE Transactions on Magnetics*, Vol. 26, No. 5, September 1990, pp. 2382-2384.

[2] D. Rodger, P.J. Leonard, J.F. Eastham, “Modelling electromagnetic rail launchers at speed using 3D finite elements”, *IEEE Transactions on Magnetics*, Vol. 27, No. 1, January 1991, pp. 314-317.

[3] E.K.C. Chan, S. Williamson, “Factors influencing the need for upwinding in two-dimensional field calculation”, *IEEE Transactions on Magnetics*, Vol. 28, No. 2, March 1992, pp. 1611-1614.

[4] T.W. Nehl, B. Lequesne, V. Gangla, S.A. Gutkowski, M.J. Robinson, T. Sebastian, “Nonlinear two-dimensional finite element modeling of permanent magnet eddy current couplings and brakes”, *IEEE Transactions on Magnetics*, Vol. 30, No. 5, September 1994, pp. 3000-3003.

[5] C.R.I. Emson, C.P. Riley, D.A. Walsh, K. Ueda, T. Kumano, "Modelling Eddy Currents Induced by Rotating Systems", *IEEE Transactions on Magnetics*, Vol. 34, No. 5, September 1998, pp. 2593-2596.

[6] S.J. Salon, *Finite Element Analysis of Electrical Machines*, Kluwer Academic Publishers, Boston, 1995.

[7] Y.Saad, *Iterative Methods for Sparse Linear Systems*, PWS Publishing Company, Boston, 1996.

[8] H. De Gersem, R. Mertens, U. Pahner, R. Belmans, K. Hameyer, "A Topological Method used for Field-Circuit Coupling", *IEEE Transactions on Magnetics*, Vol. 34, No. 5, September 1998, pp. 3190-3193.

[9] R. De Weerdt, U. Pahner, R. Belmans, E. Tuinman, “A combined finite element-circuit model of a squirrel cage induction motor”, *Proceedings of the International Conference on Electrical Machines (ICEM96)*, Vol. 3, Vigo, Spain, September 1996, pp. 63-67.

[10] K. Eriksson, D. Estep, P. Hansbo, C. Johnson, *Computational Differential Equations, Cambridge*, Cambridge University Press, 1996.

[11] A. Quarteroni, A. Valli, *Numerical Approximation of Partial Differential Equations*, Berlin: Springer-Verlag, 1994.

[12] H. De Gersem, H. Vande Sande, K. Hameyer, "Motional magnetic finite element method applied to high speed rotating devices", *9th International Symposium on Electromagnetic Fields-ISEF''99*, Pavia, Italy, September 23-25, 1999, pp. 228-231.

[13] H. Vande Sande, H. De Gersem, K. Hameyer, "Finite Element Stabilization Techniques for Convection-Diffusion Problems", to be published in *International Journal of Theoretical Electrotechnics*, 1999.

[14] U. Pahner, R. Belmans, K. Hameyer, "Optimizing ferromagnetic characteristics to reduce Newton iterations", *COMPEL*, Vol. 18, No. 4, 1999, pp. 629-637.

[15] K. Hameyer, R. Mertens, U. Pahner, R. Belmans, "New technique to enhance the accuracy of 2-D/3-D field quantities and forces obtained by standard finite-element solutions", *IEE Proc.-Sci. Meas. Technol.*, Vol. 145, No. 2, March 1998, pp. 67-75.